All-Surface Induction Heating With High Efficiency and Space Invariance Enabled by Arraying Squircle Coils in Square Lattice

Veli Tayfun Kilic, *Member, IEEE*, Emre Unal, Namik Yilmaz, and Hilmi Volkan Demir, *Senior Member, IEEE*

***Abstract*—This paper reports an all-surface induction heating system that enables efficient heating at a constant speed all over the surface independent of the specific location on the surface. In the proposed induction system, squircle coils are placed tangentially in a two-dimensional square lattice as opposed to commonly used hexagonal packing. As a proof-of-concept demonstration, a simple model setup was constructed using a 3×3 coil array along with a steel plate to be inductively heated. To model surface heating, a set of six locations for the plate was designated considering symmetry points. For all of these cases, power dissipated by the system and the plate's transient heating were recorded. Independent from the specific plate position, almost equal heating speeds were measured for the similar levels of dissipated energies in the system. Using full three-dimensional electromagnetic solutions, the experimental results were also verified. The findings indicate that the proposed system is proved to enable energy efficient space-invariant heating in all-surface induction hobs.**

***Index Terms*—Coils, electromagnetic induction, energy efficiency, inductive power transmission.**

I. Introduction

ALTHOUGH induction theory of M. Faraday goes back to the 19th century [1], its application to consumer electronics such as induction heating [2] and wireless charging systems [3]–[6] is relatively recent, which have been becoming increasingly more popular. Today domestic heating is one important application area where induction systems are widely used. Because of its safety, cleanliness, controlled and quick warming capability, and high efficiency properties, induction hobs are commonly used in the developed countries [7], [8]. Conventional induction heaters typically use large coils mounted beneath the surface. However, for efficient heating, vessels should have sizes and shapes similar to those of the coils and they should be placed right on top of the coils. To overcome this issue and provide user flexibility, all-surface induction heating has been introduced.

In all-surface induction hobs, an array of small coils is used. Working principle of all-surface induction relies on detecting a vessel and powering only the corresponding coils loaded by the vessel. For driving these coils in an efficient way, different control topologies have been reported [9]–[11]. However, most of these all-surface designs [12], [13] employ arrays of the conventional circular coils. Coils with different shapes including square and rectangular coils have also been considered for all-surface induction heating [14]. As was demonstrated previously [15], interaction between coils having rounded shapes is not as strong as that between square or rectangular coils. Although such strong interaction between side-by-side placed coils is highly desired for efficient all-surface heating, destructive coupling between diagonally located coils is undesired. Therefore, in most of the systems coils are stacked densely regardless of uniform heating all over the surface. As a result, heating with high efficiency and space invariance, which is not dependent on vessel position in the all-surface induction hob, is still an unresolved problem today.

In the previous literature, to the best of our knowledge, there have been no reports investigating the induction heating of a load placed at various locations on a hob surface. Although there is a study about flexible cooking zone [16], the proposed method is not feasible for all-surface induction heating because in the study mobile coils are offered for uniform heating of different loads. In addition, in another study [17] a method is introduced to manage heat distribution in zone-control induction heating. However, the proposed method is used for controlling power inverters of concentric coils, thus it is again not useful for all-surface induction hobs. To this end, in this paper we systematically studied an all-surface induction heating system and comparatively measured the heating efficiency and speed of the system for all possible loading positions. With our proposed system design, space-invariant

Manuscript received April 4, 2018; revised June 28, 2018; accepted July 19, 2018. Date of publication July 25, 2018; date of current version September 24, 2018. This work was supported in part by Arcelik A.S. and in part by Industry Theses Program SAN-TEZ 1463-STZ-2012-2. *(Corresponding author: Veli Tayfun Kilic.)*

V. T. Kilic was with the Department of Electrical and Electronics Engineering, Bilkent University, 06800 Ankara, Turkey. He is now with the Department of Electrical and Electronics Engineering, Abdullah Gül University, 38080 Kayseri, Turkey (e-mail: tayfun.kilic@agu.edu.tr).

E. Unal is with the Institute of Materials Science and Nanotechnology, Bilkent University, 06800 Ankara, Turkey (e-mail: unale@bilkent.edu.tr).

N. Yilmaz is with Power Electronics Department, Arçelik Company (Arcelik Tuzla Campus), 34950 Istanbul, Turkey (e-mail: namik.yilmaz@arcelik.com).

H. V. Demir is with the Department of Electrical and Electronics Engineering, Bilkent University, 06800 Ankara, Turkey, also with the Department of Physics, Bilkent University, 06800 Ankara, Turkey, also with the Institute of Materials Science and Nanotechnology, Bilkent University, 06800 Ankara, Turkey, also with the School of Electrical and Electronic Engineering, Nanyang Technological University, Singapore, and also with the School of Physical and Mathematical Sciences, Nanyang Technological University, Singapore (e-mail: volkan@bilkent.edu.tr).

Color versions of one or more of the figures in this paper are available online at http://ieeexplore.ieee.org.

Digital Object Identifier 10.1109/TCE.2018.2859627

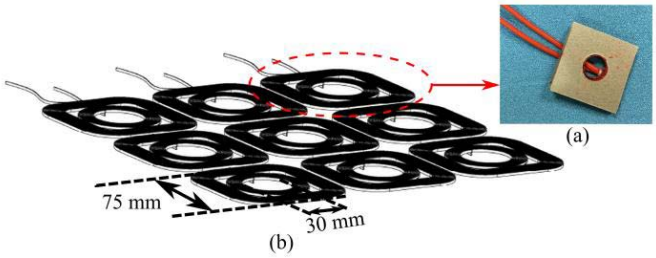

Fig. 1. (a) Photograph of a single coil designed as a repeating unit in the 3×3 coil array system from top view, (b) perspective view of the 3×3 tangent outer squircle-inner circular coil array structure in square lattice alignment and the coil's geometrical parameters.

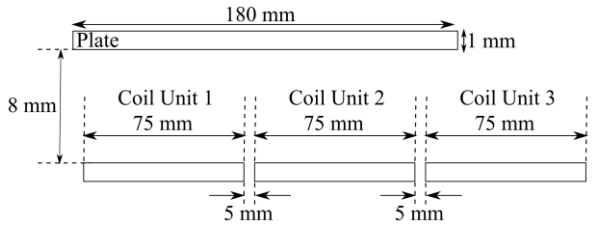

Fig. 2. Schematic of the designed system from side view together with geometrical parameters. To reflect ratio between the coils' and the plate's sizes more clearly, here plate is located to cover two coil units completely.

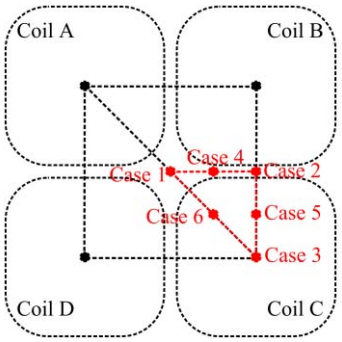

Fig. 3. Plate's center positions with respect to coils for six different measurement scenarios.

all-surface induction heating at an almost constant speed and efficiency level is demonstrated.

Here we designed, constructed, and characterized our all-surface induction heating system made of squircle coils tangentially placed in a two-dimensional (2D) square lattice. We experimentally compared the heating speed of this system in time and with dissipated energy for a plate placed at various locations on the surface. Also, with simulations we verified the results and demonstrated high efficiency of the system. This system is proved to heat loads efficiently all over its surface with a constant speed independent from the load position.

II. Design and Experimental Setup

In this study, we used coils that we prepared in the outer squircle-inner circular architecture. In the system, we aligned the coils in a square lattice creating a 180° phase difference between consecutive coils during system construction by simply reversing tips of the coils and allowing current flows to be in opposite directions. As a result, in operation, in one coil current flow is in clockwise direction and in the neighbor coil it is in counterclockwise direction, or vice versa.

The inset (Fig. 1(a)) in Fig. 1 shows a photograph of a single coil unit from top view. In this coil, after 26 turns, squircle windings at the outer rim evolve into fully circular inner turns, which is a similar structure as in the previous work investigating the phase difference effect between only two of them [15]. Here we built 9 of these coils to study the space variance of induction heating in an array. For this purpose, these units are placed tangentially in 2D square lattice to construct the 3×3 coil array structure. Fig. 1(b) shows our 3×3 tangent coil array structure in square lattice alignment from perspective view together with its geometrical parameters. Here, with long tangential sides the outer squircle windings improve couplings between side-by-side placed coils in the array. Side-by-side placement of coils in close packing increases constructive coil interactions, especially when 180° phase difference is applied. However, in the square lattice diagonal coils have in-phase currents both for 0° and 180° phase difference applications. Rounded corners of the squircle geometry thus make diagonal coils farther away from each other and decrease their destructive coupling. In the manufacturing stage, the outer squircle-inner circular shape planar coils are sandwiched between two mica layers. Since mica is resistant to high temperature, it is commonly used in such heating applications. The upper mica layer can be seen in the inset (Fig. 1(a)). In our prototype, the mica layer has a thickness of 0.40 mm. Also, there are ferrite sticks placed symmetrically around the coil center with 45° angular intervals between two consecutive sticks below the bottom mica layer, which are used for efficiency enhancement. Ferrites speed up the vessel heating by reversing the magnetic flux produced by the coils in lower half space [18], [19].

In our system the coils are placed as close as possible with 5 mm distances between them. The distance between the coils arises because of the constant side lengths of the hob surface. Heating surface is desired to be uniformly occupied by the coils but number of the coils is limited by the power circuitry. A steel plate (AISI 430) is placed above the coils. It has a cylindrical shape with 180 mm diameter and 1 mm thickness. It is important to set the plate's diameter to be equal to or larger than the side length of the repeating unit in the coil array, which is 80 mm (75 mm + 5 mm) here, for catching hot and cold spots that occur as a result of constructive and destructive coupling of the coils, respectively. Also, the distance between the plate's bottom surface and the coil units is set to 8 mm to model the thermal isolation material (such as Silargan glass) on the hob surface. A schematic of the designed system from side view together with geometrical parameters is illustrated in Fig. 2.

Projection coverage of the coils by steel plate depends on the plate position. Therefore, different coils might be powered up and heating of the plate may differ depending on its location on the hob surface. To observe these variations, measurements were conducted for the plate's six different placements. Positions of the plate's center with respect to coils for these six scenarios are shown in Fig. 3.

In the figure, positions of the plate's center for six different cases are marked with red dots. In Case 1 and Case 2 plate

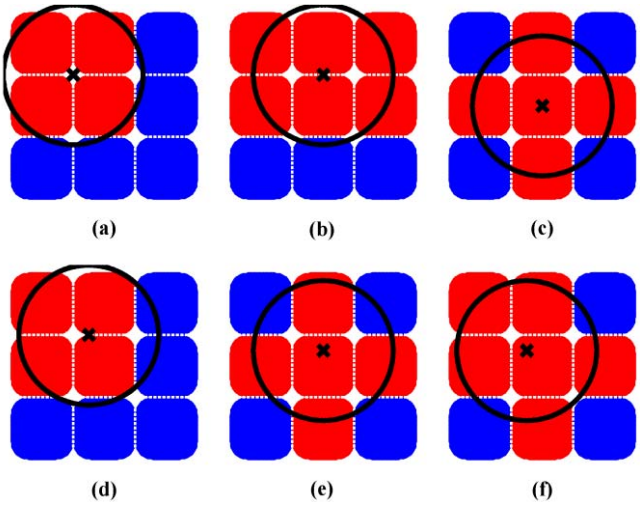

Fig. 4. Placements of the plate and the on- and off-coils in six different scenarios. Here, (a), (b), (c), (d), (e), and (f) subtitles correspond to Case 1, Case 2, Case 3, Case 4, Case 5, and Case 6 in Fig. 3, respectively. The red coils correspond to the turned-on ones, and the blue, to the turned-off ones.

is located to be in the middle of Coil A – Coil C and Coil B – Coil C pairs, respectively. Also, in Case 3 plate's center and the center of the third coil (Coil C) are on top of each other. In other cases, i.e., Case 4, Case 5, and Case 6, plate's center is positioned to be at the middle of the positions in Case 1, Case 2, and Case 3. Because of symmetry only four coils are represented. Note that coils are aligned tangentially in square lattice thus coil centers construct a square. Similarly, points indicating positions of the plate's center for measurement cases construct a triangle. Again, because of symmetry other measurements outside the red triangular area would yield similar results. Here, the highest distance between two consecutive positions of the plate's center is approximately 28.28 mm (distances between Case 1 – Case 6, Case 2 – Case 6, and Case 3 – Case 6). The number of measurement scenarios can be increased further. However, results obtained with the new scenarios would be amid the results of the six cases mentioned above (Case 1, Case 2, Case 3, Case 4, Case 5, and Case 6). Also, the distance between the plate's center positions in possible new scenarios and in the existing cases can be 14.14 mm at maximum. This distance is very small compared to the plate's diameter. Therefore, six measurement scenarios are enough to understand the plate's heating variation with its position.

For each case, areas of the coils covered by the plate were calculated. Based on L-R measurements data reported for vessel detection [20], coils whose at least 30% of the area is covered by the plate were decided to be powered up. Fig. 4 shows placements of the coils and the plate for all the measurement cases showing turned-on and turned-off coils. In the figure, the plate's circumference and center are represented with black circle and 'x' marker, respectively. Similarly, on- and off-coils are pointed out with red and blue colors, respectively.

For each case in Fig. 4, measurements were repeated. In our measurements, a commercially available electronic card was used as a power supply circuitry that converts 50 Hz city line signal to a 50 KHz frequency signal. Resultantly, corresponding coils in each case were connected to and driven by the outputs of the supply circuitry at a frequency of 50 KHz. Voltage and current signals supplied to and driven by each coil were measured instantaneously by means of an oscilloscope with help of a voltage probe and a current clamp, respectively, while continuously recording amplitudes of the signals and phase between them. Total real power supplied to the coils, which is the true power, was calculated from the measured voltage and current signals. The power calculation is given by (1). In addition, equivalent resistance and inductance of the coils were also calculated from the measured voltage and current signals. They are formulated in (2) and (3).

$$P_{rms} = |V_{rms}||I_{rms}| \cos \varnothing \tag{1}$$

$$R_{eq} = \frac{|V_{rms}|}{|I_{rms}|} \cos \varnothing \tag{2}$$

$$L_{eq} = \frac{1}{\omega} \frac{|V_{rms}|}{|I_{rms}|} \sin \varnothing \tag{3}$$

Here P_{rms} is the true rms power (W). R_{eq} and L_{eq} are the equivalent resistance (Ω) and inductance (H), respectively. V_{rms} and I_{rms} are the rms voltage (V) and current (A), respectively. Also, ω is the angular frequency and $\varnothing$ is the phase difference between the voltage and current signals.

We calculated the plate's temperature change with total dissipated energy in the system. Total dissipated energy in the system is found by taking integral of the total instantaneous true power supplied to the coils over time. Relation between the dissipated energy and the true power is given by (4)

$$E_{total} = \int P_{rms} \cdot dt \tag{4}$$

where E_{total} is the total dissipated energy in the system (J) and P_{rms} is the instantaneous true power supplied to the coils (W).

The plate's temperature was measured and recorded using a thermal camera. In the constructed measurement setup a thermal camera was placed above the plate where coils heat the plate from its bottom side. Used camera has $25° \times 19°$ field of view and its distance to the plate was adjusted such that the plate is fully inside the camera's field of view. In addition, with additional lenses thermal camera was focused on the plate with a resolution on the plate to be finer than 1 mm$\times$1 mm. Temperature distribution over the plate's top surface was instantaneously measured. Since temperature distribution is not uniform, we calculated the plate's average temperature by integrating the temperature distribution over the top surface and divided the result by the surface area. Because the plate's thickness is so thin (1 mm) and the camera was placed above the plate, in the calculation temperature gradient between the plate's bottom and top surfaces is ignored.

III. Modeled System and Simulation Method

For comparison purposes, we also modeled and simulated the system using three-dimensional (3D) electromagnetic solver. The constructed system is illustrated in Fig. 5 from top and side views. The system is exactly the same with the one built in experiments (see Fig. 2) except for the ferrite

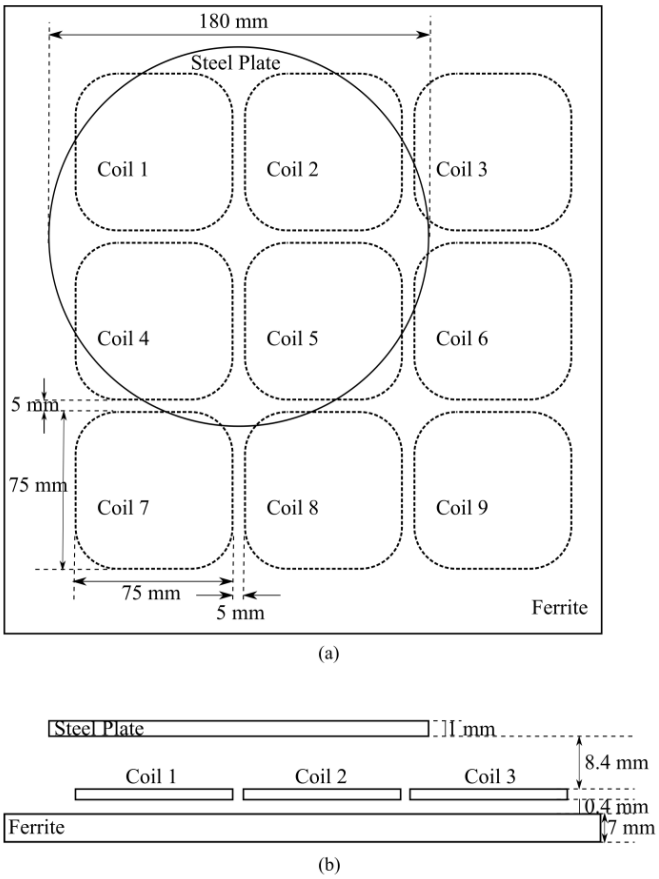

Fig. 5. Schematic of the modeled system from (a) top view and (b) side view together with geometrical parameters. Here, the plate is positioned above the coils as in Case 1.

layer below the coils. Instead of placing ferrite sticks underneath each coil, ferrite layer is located under the coils to cover the whole plane. This makes the modeled system simpler and allows for fast convergence of numerical simulations. In the system, ferrite layer has 7 mm thickness and the distance between bottom surface of the coils and top surface of the ferrite layer is set to 0.40 mm, which is the same with the thickness of the mica layer in our manufactured coil prototypes (see Fig. 1(a)). In the simulations, ferrite layer was modeled to be made of Mn-Zn and mica layers were replaced with free space. Nine of the outer squircle-inner circular shape coils are stacked in square lattice to construct a 3×3 tangent coil array structure. Coils have exactly the same shape with the coils used in measurements such that they have 30 mm inner diameter and 75 mm side lengths. In addition, coils were modeled to be made of perfect electrical conductor (PEC). Since prototyped coils are composed of litz strands, in our simulations by modeling coils with PEC we force currents to flow across entire cross section of coil windings. The tangential distance between the coils is set to 5 mm to be exactly the same as the coil distances in the measurement setup. A cylindrical shape steel plate having 1 mm thickness and 180 mm diameter is located 8.40 mm above from the coils' top surface. The distance between the plate and the coils (8.40 mm) includes the distance between the plate's bottom surface and the coil units (8 mm) and the thickness of the mica layer (0.40 mm) in our measurement system (see Fig. 2). Simulations were repeated varying the plate's position in the first three cases, i.e., Case 1, Case 2, and Case 3.

In our simulations, each coil was driven by a separate current source with the specific amplitude determined in measurements. In addition, phase difference between current signals supplied to consecutive coils was set to 180°, which is the same within our measurements. In the simulations, because of their complex 3D geometries having rounded edges, coils and the plate were meshed with tetrahedron shape meshes having maximum sizes to be smaller than 2 mm and 5 mm, respectively. In addition, open boundary conditions were set in all directions to model free space and minimize reflections from the boundaries. The simulations were run at 50 KHz frequency, which is the same within the measurements. In the simulations, we calculated total power transferred to and dissipated on the plate as ohmic loss.

IV. Results and Discussion

We initially conducted measurements for each case. In all experiments 180° phase difference was applied to consecutive coils. For instance, in Case 1 (Fig. 4(a)) among four working coils two diagonally located coils have currents flowing in one (e.g., in clockwise) direction and the other two cross coils have currents flowing in the opposite (e.g., in counter clockwise) direction.

Heating of the plate was observed with help of the thermal camera. As an exemplary, Fig. 6 shows the temperature distributions over the steel plate's top surface (at 55 s after power was turned on) for all the cases.

In the figure, to represent coil locations, boundaries between the coils are marked with dotted lines. As seen, the plate is heated starting from the regions above the adjacent coils' close sides. This is because of the 180° phase difference between the consecutive tangential coil currents. On the other hand, temperature increases are slower in areas above the coils' corners, where cross coils are being the closest. This is because of cross coils' having currents in the same direction, i.e., 0° phase difference between. This is one of the reasons why outer rim of the coils were selected to be squircle shape instead of square. By rounding corners of the square shape, destructive interaction between cross coils is aimed to be decreased. In the figure, temperature distributions obtained in Case 1, Case 2, and Case 3 are almost symmetric with respect to the plate's center. This is expected and based on the plate's placements with respect to the on-coils such that the plate is located in the middle of the four adjacent tangential on-coils in Case 1, six neighbor tangential on-coils in Case 2, and five symmetric and adjacent tangential on-coils in Case 3 (see Figs. 4(a), (b), and (c)). Small heating variations that violate complete symmetry, such as the high temperature area between the two adjacent tangential upper coils in Case 1, are due to measurement error of the plate's not being completely parallel to the coils' top surfaces. Coupling between a coil and a load is strongly related with their separation. In the system since coils and the plate are close to each other only with 8 mm

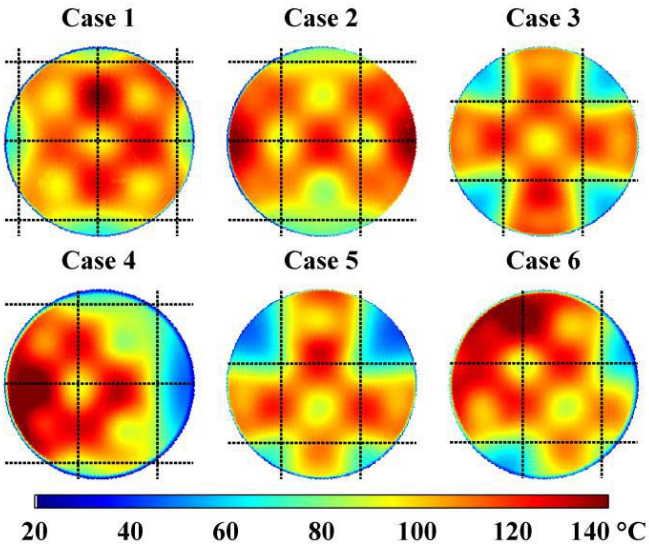

Fig. 6. Temperature distributions over the plate's top surface at 55 s after the power was turned on for all the cases.

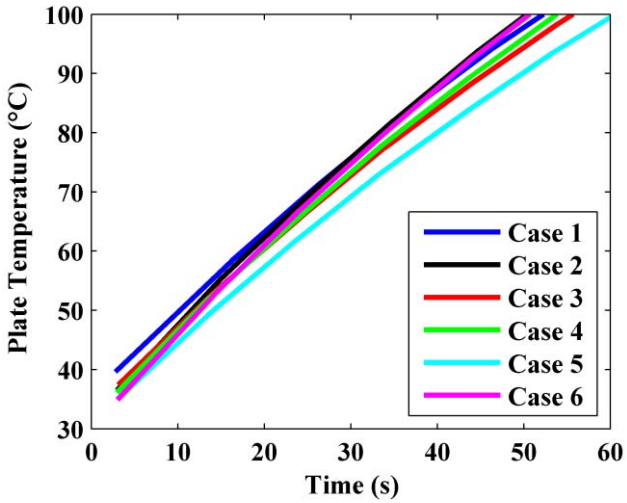

Fig. 7. Average temperature changes over the plate with time for all the measurement cases.

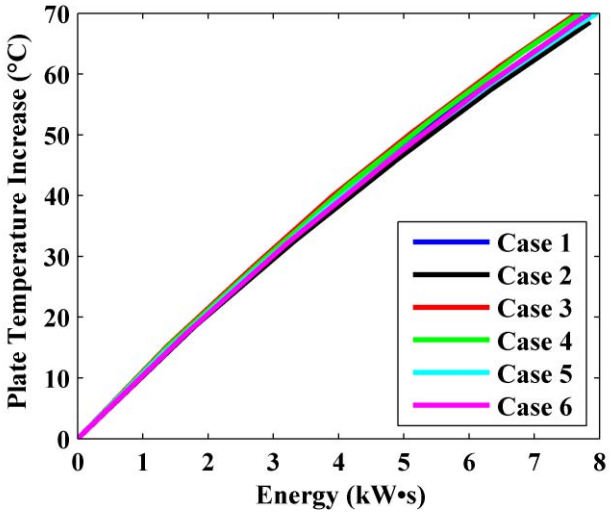

Fig. 8. Average temperature changes over the plate with total dissipated energy in the system for all the measurement cases.

distance, small changes in the coil-plate separations violate absolute symmetry.

Fig. 7 shows changes of average temperature over the plate with time. The nonzero initial times in the figure are because of the time required for the thermal camera's connection and taking of the image.

In our measurements, the plate was heated up till its average temperature passes 100 °C. In the figure, at high temperatures more time is required to heat up the plate further. In other words, temperature increase decelerates as time goes on. This can be explained with high temperature gradient between the plate and the medium, which causes rapid cooling of the plate.

In addition, in Fig. 7 plate's heating speed is very similar for all the cases. It is important for comparison of the system's heating efficiencies with a plate at different positions. However, heating speed depends on supplied power, too. Therefore, change of the plate's temperature with total dissipated energy in the system was calculated and is presented in Fig. 8.

The heating is almost the same for all the cases in the figure. This is expected because real power was supplied to the coils in a close range in all the measurements. Also, in the figure decrease in the plate's heating speed is observed, too. Plate's similar heating for all the cases in Fig. 8 indicates that the system's heating efficiency and speed are independent of the plate position. In other words, the proposed all-surface induction heating system heats a vessel efficiently and quickly all over its surface.

Fig. 9 shows change of the plate's heating speed with its temperature for all the measurement cases. Heating speed is calculated by taking slope of the curves in Fig. 8. Here markers denote the calculated heating speeds and lines are the corresponding first order fittings. In the figure, decrease in the plate's heating speed is clearly seen. For instance, with 1 kW·s input energy the plate's temperature increased more than 10.0 °C if its temperature was around 40 °C, but if its temperature was around 110 °C than with 1 kW·s input energy the plate's temperature increased at most 7.0 °C in our system. In addition, in the figure at a constant plate temperature the difference between temperature increase speeds for the cases is at most 0.9 °C/(kW·s). This is expected from Fig. 8 and supports the result of space-invariant heating of the system.

We further investigated the real powers supplied to each coil and their equivalent resistance and inductance values. The average real powers supplied to each coil and their sum over 50 seconds are given in Table I for the first three cases. In the table off-coils are indicated with X. Also, coils are called starting from left top towards the right bottom in ascending order. For instance, the left top coil in Fig. 4 is called Coil 1. Similarly, the right top, the left bottom, and the right bottom coils are called Coil 3, Coil 7, and Coil 9, respectively, in the table.

As seen, powers supplied to the coils in each case are proportional with their loadings. For example, in Case 1 supplied

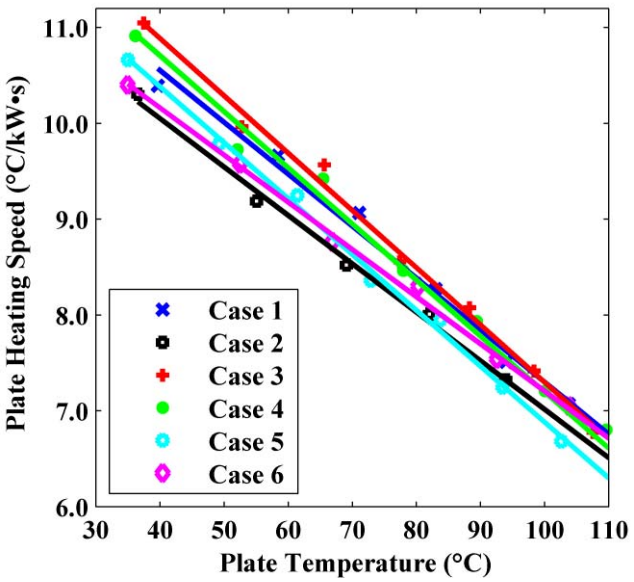

Fig. 9. Change of the plate temperature increase speed in the system with the plate temperature for all the measurement cases.

TABLE I
AVERAGE REAL POWERS SUPPLIED TO AND DISSIPATED BY THE COILS AND THEIR SUM

	Case 1	Case 2	Case 3
Coil 1	33.14 W	20.50 W	X
Coil 2	32.31 W	38.20 W	21.96 W
Coil 3	X	15.71 W	X
Coil 4	35.45 W	19.36 W	21.95 W
Coil 5	32.02 W	39.28 W	42.66 W
Coil 6	X	18.05 W	20.37 W
Coil 7	X	X	X
Coil 8	X	X	19.84 W
Coil 9	X	X	X
Total	132.92 W	151.10 W	126.78 W

powers to the coils are almost the same because of their equal loading by the plate. Similarly, supplied powers to Coil 2 and Coil 5 are the highest in Case 2 because they were covered by the plate most largely. Again, Coil 5 was covered by the plate most largely and thus its supplied power is the highest in Case 3. On the other hand, differences between total powers in the table are because of different loadings of the off-coils in the cases. As loading of the off-coils increases, total supplied power decreases and vice versa. For instance, among the first three cases, total area of the off-coils covered by the plate is the largest in Case 3, whereas it is minimum in Case 2.

Although typical induction heating systems for cooktops are suitable to deliver more power to a similar load, in the system small power levels of 16 to 43 W are supplied to each coil with a total dissipated power between 127 and 151 W to clearly observe and record heating of the plate. Otherwise, because of quick heating, it might be difficult to detect high and low temperature areas on the plate (see Fig. 6).

Moreover, variations in the equivalent resistance and inductance of each coil for the first three cases are shown in Fig. 10 together with the variations in the measured currents on the coils. In the subfigures (Figs. 10(a), (b), (d), (e), (g), and (h)), the measured resistance and inductance values are pointed out with markers and their averages are indicated with lines having the same color with the markers in the corresponding cases.

In Figs. 10(a), (d), and (g), equivalent resistance values measured on the coils are found to be proportional with their loadings. For example, in Case 2 (Fig. 10(d)) resistance values of Coil 2 and Coil 5 are considerably higher than those of the other on-coils. Similarly, in Case 3 (Fig. 10(g)) resistance of Coil 5 is the highest. On the other hand, in Case 1 (Fig. 10(a)) resistance values are much closer to each other than in other cases. These results are expected because equivalent resistance of a coil relates to total real power supplied to and dissipated on the coil, which includes power that heats up the coil, power transferred to the plate, and other loss powers. Therefore, measured resistance values in Figs. 10(a), (d), and (g) exhibit similar behavior with those of the real power supplied to and dissipated on the coils that are given in Table I. In Figs. 10(b), (e), and (h), on the other hand, inductance values do not show similar trend. Inductance values are close to each other and they are found to be related with currents (as will be further explained later using measured current values in Figs. 10(c), (f), (i), and Table II). Experiments were repeated at different frequencies and similar results were obtained.

Furthermore, to verify the results we studied the system using full 3D electromagnetic solutions. To construct the same setup in the numerical simulations with that in the measurement cases, we first found the average currents supplied to the coils from measured current signals. For the first three cases, i.e., Case 1, Case 2, and Case 3, variations in the measured currents on the coils are shown in Figs. 10(c), (f), and (i). In the figure, currents on the coils are almost constant in time. Small decreases in the current amplitudes result from the fact that as the system equivalent inductance diverges from its initial value system resonance frequency deviates, too. In other words, with changes in inductance in time system resonance frequency shifts away from 50 KHz operational frequency. Currents supplied to the coils on average are given in Table II. Similar to Table I, here off-coils are again indicated with X.

If we compare the results shown in Figs. 10(b), (e), and (h) with those represented in Figs. 10(c), (f), and (i) and given in Table II, it is seen that there is an inverse relation between the equivalent inductances of the coils and the currents supplied to them. For instance, in Case 1 equivalent inductance of Coil 1 is the lowest and the other on-coils have equivalent inductance values close to each other (Fig. 10(b)), while the current supplied to Coil 1 is much higher than the currents supplied to the other coils in Case 1 (Fig. 10(c)). Similarly, equivalent inductance value of Coil 1 is much lower than that of other on-coils in Case 2 (Fig. 10(e)) and equivalent inductance value of Coil 5 is much higher than equivalent inductance of the other on-coils in Case 3 (Fig. 10(h)),

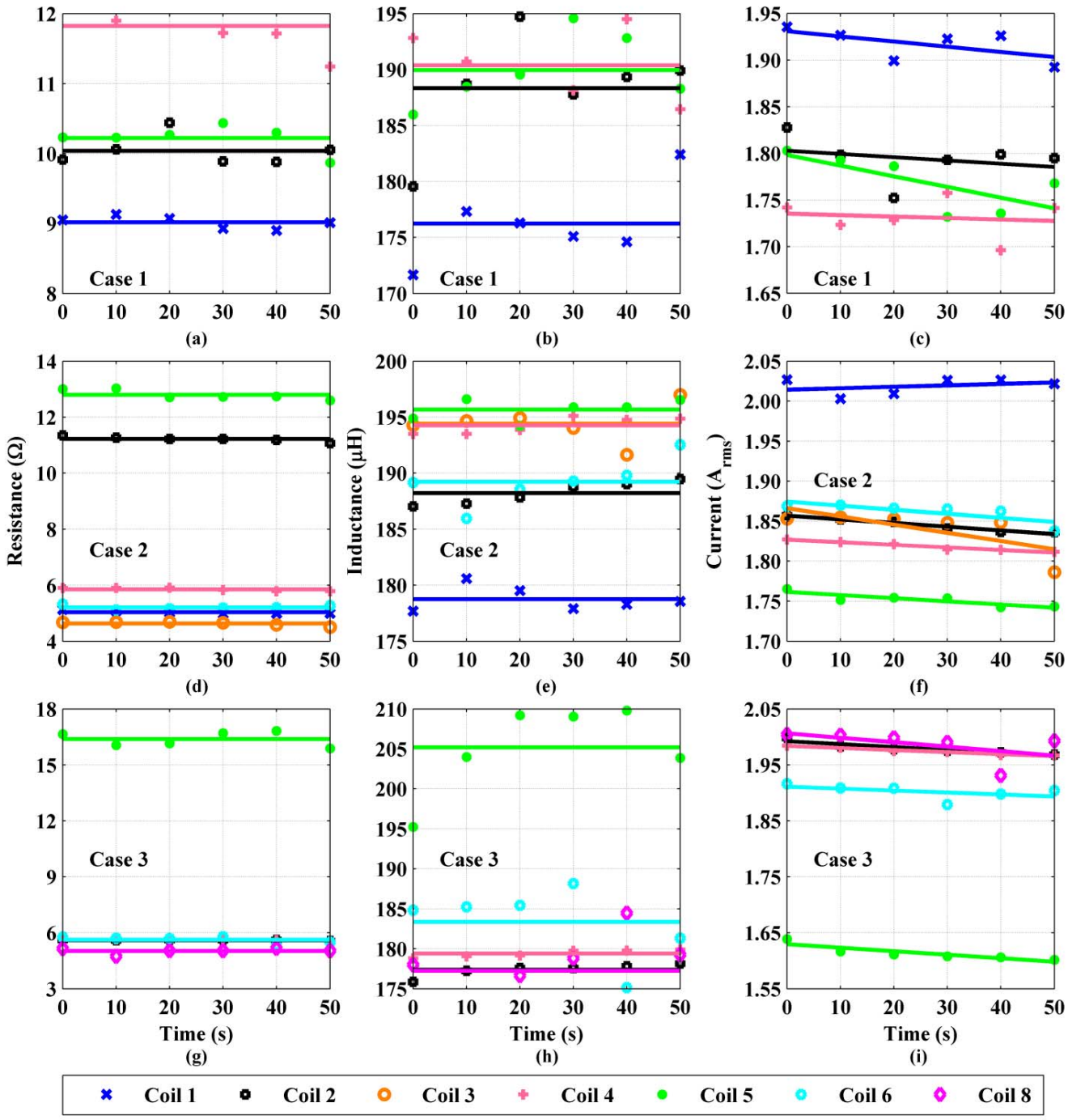

Fig. 10. Variations in the equivalent resistance ((a), (d), (g)) and equivalent inductance ((b), (e), (h)) of the coils together with the measured currents on the coils ((c), (f), (i)) over time for three different scenarios: (a)-(c) Case 1, (d)-(f) Case 2, and (g)-(i) Case 3. Here markers denote the measured resistance, inductance, and current values. In addition, lines indicate averages of the measured values in each case in resistance and inductance plots, whereas lines represent the corresponding first order fittings of the measured currents in current plots.

whereas current supplied to Coil 1 is the highest in Case 2 (Fig. 10(f)) and current supplied to Coil 5 is the lowest in Case 3 (Fig. 10(i)).

In simulations, total power transferred to and dissipated on the plate was calculated as 130.37 W, 161.52 W, and 148.49 W for Case 1, Case 2, and Case 3, respectively. On the other hand, in Table I, total power supplied to the coils, which is the total dissipated power in the coils and the plate, was found as 132.92 W, 151.10 W, and 126.78 W. Since the prototyped coils in experiments consist of several litz strands, it would be a fair assumption to ignore power dissipated on coils for their self-heating. In other words, most of the total power supplied to the coils in Table I is the power transferred to the plate. Therefore, it can be deduced that the calculated powers in the simulations and the measured powers in the experiments are close to each other.

TABLE II
AVERAGE CURRENTS SUPPLIED TO THE COILS

	Case 1	Case 2	Case 3
Coil 1	1.92 A	2.02 A	X
Coil 2	1.79 A	1.85 A	1.97 A
Coil 3	X	1.84 A	X
Coil 4	1.73 A	1.82 A	1.97 A
Coil 5	1.77 A	1.75 A	1.61 A
Coil 6	X	1.86 A	1.90 A
Coil 7	X	X	X
Coil 8	X	X	1.98 A
Coil 9	X	X	X

TABLE III
CALCULATED POWERS TRANSFERRED TO AND DISSIPATED ON THE PLATE

Used Coils	Phase Difference Between Coils	Case Number	Transferred Power
Squircle Coils	0°	Case 1	101.21 W
		Case 2	107.53 W
		Case 3	121.42 W
	180°	Case 1	130.37 W
		Case 2	161.52 W
		Case 3	148.49 W
Circular Coils	0°	Case 1	105.65 W
		Case 2	116.68 W
		Case 3	127.81 W
	180°	Case 1	119.45 W
		Case 2	145.27 W
		Case 3	140.49 W

Furthermore, for comparison purposes, system simulations were repeated with 0° phase difference between coils and using conventional circular coils. In these simulations, squircle coils in the modeled system (see Fig. 5) were replaced with nine conventional circular shaped coils. Calculated powers transferred to the plate in the systems are listed in Table III.

In the table, in all the cases the highest transferred power is found in the system where the squircle coils are driven by the currents of 180° phase difference between adjacent coils. This demonstrates the advantages of applying phase difference and using array of outer squircle coils instead of conventional circular coils in the designed system. In addition, transferred powers are found to be in close ranges for the cases in all the systems. This is expected and supports the result of space-invariant heating in systems where coils are aligned in a 2D periodic square lattice. The proposed squircle shaped coils' alignment in square lattice allows enhanced interaction and coupling because of the coils' unique geometry and phase difference application together with space-invariant heating which occur as a result of the plate's catching cold and hot spots.

Small differences between the powers measured in experiments and calculated in simulations for the designed system that are given in Table I and Table III, respectively, might arise because of finite measurement precision, i.e., measurement errors occur during instantaneous recording of voltage and current signals together with their parameters, and limited simulation accuracy that occurs as a result of finite meshing of the system. Also, another important reason that causes differences between the calculated and the measured powers is the fact that in the simulations coils are driven by separate current sources with constant amplitudes, whereas in measurements currents supplied to the coils vary in time.

V. CONCLUSION

In this paper a new all-surface induction hob design is introduced. In the proposed system, an array of tangential outer squircle coils is aligned in a 2D square lattice. For plate's various placements heating speed of the design was measured and results were compared. In experiments, plate's heating with an almost constant speed in time was obtained for the plate's various positions on the hob surface. In addition, plate's heating speed was calculated as a function of the dissipated energy in the system. Plate's temperature increase with total dissipated energy was found almost the same for all the cases, where the difference was calculated to be at most 0.9 °C/(kW·s) for the used plate at a constant temperature. Results indicate that the heating speed and efficiency of the proposed system are fairly independent from the plate's location on the hob surface. Moreover, in experiments, plate's heating speed was observed to be decelerated with its temperature, which is expected from the increased temperature gradient between the plate and the medium. Also, for different cases power levels supplied to and dissipated on each coil were measured. In the system, true power supplied to each coil is shown to be proportional with their loadings. Furthermore, equivalent resistance and inductance of the coils were measured. Equivalent resistances of the coils are found to be proportional with their loadings, whereas inductances of the coils are discovered to be related with the currents driven. The results were verified with full 3D electromagnetic simulations.

This study demonstrates the feasibility of all-surface induction hobs with high efficiency and uniformity. Also, space-invariant heating all over the surface with high efficiency at a constant speed is an important feature of the proposed system essential to wide penetration of all-surface induction hobs in the market. The designed system is the first in its field for enabling users complete flexibility in terms of all-surface heating and the study is different from other literature works in terms of investigating the designed system parameters for a load's various placements all over the surface. Further extension of this work will include enhancing efficiency and speed of the system using 3D arrangement of the coils.

ACKNOWLEDGMENT

The authors would like to thank Erdal Gonendik for his assistance in earlier coil design work and Berkay Bozok for his assistance in part of characterization studies.

REFERENCES

[1] A. Mühlbauer, *History of Induction Heating and Melting*. Essen, Germany: Vulkan-Verlag, 2008.

[2] T. Tanaka, "A new induction cooking range for heating any kind of metal vessels," *IEEE Trans. Consum. Electron.*, vol. 35, no. 3, pp. 635–641, Aug. 1989, doi: 10.1109/30.44329.

[3] J. Moon, H. Hwang, B. Jo, H.-A. Shin, and S.-W. Kim, "Design of a 5-W power receiver for 6.78 MHz resonant wireless power transfer system with power supply switching circuit," *IEEE Trans. Consum. Electron.*, vol. 62, no. 4, pp. 349–354, Nov. 2016, doi: 10.1109/TCE.2016.7838086.

[4] V. T. Nguyen, S. H. Kang, J. H. Choi, and C. W. Jung, "Magnetic resonance wireless power transfer using three-coil system with single planar receiver for laptop applications," *IEEE Trans. Consum. Electron.*, vol. 61, no. 2, pp. 160–166, May 2015, doi: 10.1109/TCE.2015.7150569.

[5] D. Dai and J. Liu, "Design of a practical human-powered contactless charger for cellphone," *IEEE Trans. Consum. Electron.*, vol. 59, no. 3, pp. 476–482, Aug. 2013, doi: 10.1109/TCE.2013.6626227.

[6] H. Hoang, S. Lee, Y. Kim, Y. Choi, and F. Bien, "An adaptive technique to improve wireless power transfer for consumer electronics," *IEEE Trans. Consum. Electron.*, vol. 58, no. 2, pp. 327–332, May 2012, doi: 10.1109/TCE.2012.6227430.

[7] O. Lucia, J. Acero, C. Carretero, and J. M. Burdio, "Induction heating appliances: Toward more flexible cooking surfaces," *IEEE Ind. Electron. Mag.*, vol. 7, no. 3, pp. 35–47, Sep. 2013, doi: 10.1109/MIE.2013.2247795.

[8] J. Acero *et al.*, "The domestic induction heating appliance: An overview of recent research," in *Proc. IEEE Appl. Power Electron. Conf. Expo. (APEC)*, Austin, TX, USA, 2008, pp. 651–657.

[9] Ó. Lucia, J. M. Burdio, L. A. Barragan, C. Carretero, and J. Acero, "Series resonant multiinverter with discontinuous-mode control for improved light-load operation," *IEEE Trans. Ind. Electron.*, vol. 58, no. 11, pp. 5163–5171, Nov. 2011, doi: 10.1109/TIE.2011.2126541.

[10] Ó. Lucia, C. Carretero, J. M. Burdio, J. Acero, and F. Almazan, "Multiple-output resonant matrix converter for multiple induction heaters," *IEEE Trans. Ind. Appl.*, vol. 48, no. 4, pp. 1387–1396, Jul./Aug. 2012, doi: 10.1109/TIA.2012.2199456.

[11] Ó. Lucia, H. Sarnago, and J. M. Burdio, "Soft-stop optimal trajectory control for improved performance of the series-resonant multiinverter for domestic induction heating applications," *IEEE Trans. Ind. Electron.*, vol. 62, no. 10, pp. 6251–6259, Oct. 2015, doi: 10.1109/TIE.2015.2417132.

[12] K. Leidig and M. Herzog, "Induction cooking hob," European Patent EP 2 265 088 B1, Jun. 27, 2012.

[13] J. Acero, C. Carretero, Ó. Lucia, R. Alonso, and J. M. Burdio, "Mutual impedance of small ring-type coils for multiwinding induction heating appliances," *IEEE Trans. Power Electron.*, vol. 28, no. 2, pp. 1025–1035, Feb. 2013, doi: 10.1109/TPEL.2012.2205270.

[14] F. Forest *et al.*, "Frequency-synchronized resonant converters for the supply of multiwinding coils in induction cooking appliances," *IEEE Trans. Ind. Electron.*, vol. 54, no. 1, pp. 441–452, Feb. 2007, doi: 10.1109/TIE.2006.888797.

[15] V. T. Kilic, E. Unal, E. Gonendik, N. Yilmaz, and H. V. Demir, "Strongly coupled outer squircle–inner circular coil architecture for enhanced induction over large areas," *IEEE Trans. Ind. Electron.*, vol. 63, no. 12, pp. 7478–7487, Dec. 2016, doi: 10.1109/TIE.2016.2594228.

[16] F. Sanz, C. Franco, C. Sagues, D. Paesa, and S. Llorente, "Flexible cooking zone with 2D mobile inductors in induction hobs," in *Proc. IEEE Ind. Electron. Soc. Conf. (IECON)*, Montreal, QC, Canada, 2012, pp. 3262–3267.

[17] H. N. Pham, H. Fujita, K. Ozaki, and N. Uchida, "Estimating method of heat distribution using 3-D resistance matrix for zone-control induction heating systems," *IEEE Trans. Power Electron.*, vol. 27, no. 7, pp. 3374–3382, Jul. 2012, doi: 10.1109/TPEL.2011.2179984.

[18] W. A. Roshen and D. E. Turcotte, "Planar inductors on magnetic substrates," *IEEE Trans. Magn.*, vol. 24, no. 6, pp. 3213–3216, Nov. 1988, doi: 10.1109/20.92379.

[19] W. A. Roshen, "Effect of finite thickness of magnetic substrate on planar inductors," *IEEE Trans. Magn.*, vol. 26, no. 1, pp. 270–275, Jan. 1990, doi: 10.1109/20.50553.

[20] V. T. Kilic, E. Unal, and H. V. Demir, "Wireless metal detection and surface coverage sensing for all-surface induction heating," *Sensors*, vol. 16, no. 3, p. 363, Mar. 2016, doi: 10.3390/s16030363.

Veli Tayfun Kilic (S'14–M'17) was born in Adana, Turkey, in 1987. He graduated from Adana Science High School, Adana, and received the B.S., M.S., and Ph.D. degrees from Bilkent University, Ankara, Turkey, in 2009, 2011, and 2017, respectively, all in electrical and electronics engineering. His research focus is high-efficiency inductive energy transfer and applications.

From 2009 to 2017, he was a Research Assistant with the Electrical and Electronics Engineering Department, Bilkent University. From 2012 to 2013, he was a Design Engineer with Mikes Company. From 2014 to 2018, he was a Researcher with TUBITAK, the Scientific and Technological Research Council of Turkey. In 2018, he joined Abdullah Gul University, Kayseri, Turkey, where he is currently an Assistant Professor with the Department of Electrical and Electronics Engineering. His research interests include radio frequency systems, near-field and far-field electromagnetic coupling, radio frequency antennas, plasmonic antennas, and radio frequency circuits.

Emre Unal received the B.S. degree in electrical and electronics engineering from Hacettepe University, Ankara, Turkey, in 2005. He is a full-time Research Engineer with the Institute of Materials Science and Nanotechnology, Bilkent University, Ankara, under the supervision of Prof. H. V. Demir, where he is researching on the development of microwave and optoelectronic devices.

Namik Yilmaz received the B.S. and M.S. degrees in electrical engineering from Istanbul Technical University, Istanbul, Turkey, in 1997 and 2000, respectively, where he is currently pursuing the Ph.D. degree in electrical engineering. He has been with the Power Electronics Group, Arcelik A.S., since 2000. His main interests include design of motor control hardware and algorithms, design of resonant inverter topologies, and coils and algorithms for domestic induction cooking and microwave heating.

Hilmi Volkan Demir (M'04–SM'11) received the B.S. degree in electrical and electronics engineering from Bilkent University, Ankara, Turkey, in 1998 and the M.S. and Ph.D. degrees in electrical engineering from Stanford University, Stanford, CA, USA, in 2000 and 2004, respectively. In 2004, he joined Bilkent University, where he is currently a Professor with joint appointments with the Department of Electrical and Electronics Engineering and the Department of Physics and is also with the Institute of Materials Science and Nanotechnology. He is also a fellow of National Research Foundation in Singapore and a Professor with Nanyang Technological University. His research interests include the development of innovative optoelectronic and RF devices.

He was a recipient of the European Union Marie Curie Fellowship, the Turkish National Academy of Sciences Distinguished Young Scientist Award, the European Science Foundation-European Young Investigator Award, and the Nanyang Award for Research Excellence.